Published in final edited form as:
Photochem Photobiol. 2010 ; 86(2): 389–396. doi:10.1111/j.1751-1097.2009.00682.x.

Ultraviolet B Light-induced Nitric Oxide/Peroxynitrite Imbalance in Keratinocytes—Implications for Apoptosis and Necrosis

Shiyong Wu[*,1,2,3], **Lei Wang**[1,2], **Adam M. Jacoby**[1], **Krystian Jasinski**[1], **Ruslan Kubant**[1], and **Tadeusz Malinski**[1,3]

[1]Department of Chemistry and Biochemistry, Ohio University, Athens, OH

[2]Edison Biotechnology Institute, Ohio University, Athens, OH

[3]Molecular and Cellular Biology Program, Ohio University, Athens, OH

Abstract

Elevation of nitric oxide ($NO^{\cdot}$) can either promote or inhibit ultraviolet B light (UVB)-induced apoptosis. In this study, we determined real-time concentration of $NO^{\cdot}$ and peroxynitrite ($ONOO^{-}$) and their role in regulation of membrane integrity and apoptosis. Nanosensors (diameter 300–500 nm) were used for direct *in situ* simultaneous measurements of $NO^{\cdot}$ and $ONOO^{-}$ generated by UVB in cultured keratinocytes and mice epidermis. An exposure of keratinocytes to UVB immediately generated $ONOO^{-}$ at maximal concentration of 190 n_M followed by NO release with a maximal concentration of 91 n_M. The kinetics of UVB-induced $NO^{\cdot}/ONOO^{-}$ was in contrast to cNOS agonist stimulated $NO^{\cdot}/ONOO^{-}$ from keratinocytes. After stimulating cNOS by calcium ionophore (CaI), $NO^{\cdot}$ release from keratinocytes was followed by $ONOO^{-}$ production. The $[NO^{\cdot}]$ to $[ONOO^{-}]$ ratio generated by UVB decreased below 0.5 indicating a serious imbalance between cytoprotective $NO^{\cdot}$ and cytotoxic $ONOO^{-}$—a main component of nitroxidative stress. The $NO^{\cdot}/ONOO^{-}$ imbalance increased membrane damage and cell apoptosis was partially reversed in the presence of free radical scavenger. The results suggest that UVB-induced and cNOS-produced $NO^{\cdot}$ is rapidly scavenged by photolytically and enzymatically generated superoxide ($O_2^{\cdot -}$) to produce high levels of $ONOO^{-}$, which enhances oxidative injury and apoptosis of the irradiated cells.

Introduction

UVB induces the production of nitric oxide ($NO^{\cdot}$), which plays a role in regulation of apoptosis in skin cells (1–5). $NO^{\cdot}$ is produced from L-arginine and oxygen in reaction catalyzed by nitric oxide synthase (NOS). The family of $NO^{\cdot}$ synthases consists of constitutive enzymes (cNOS), including neuronal (nNOS) and endothelial NOS (eNOS), and inducible $NO^{\cdot}$ synthase (iNOS). The activation of cNOS could be immediately triggered by elevation of the intracellular calcium level, which induces the binding of calmodulin to the inactive cNOS (6–8). The induction of iNOS is regulated through multiple signaling pathways and it could take hours to increase the expression of iNOS (9).

Most cell types residing in the skin have been reported to produce $NO^{\cdot}$ in response to appropriate stimulation. Keratinocytes (10), Langerhans cells (11), dermal fibroblasts (12), melanocytes (13) and melanoma (14) cells express iNOS upon stimulation with inflammatory cytokines. Among these cells, keratinocytes account for 90–95% of total cells in the epidermis. Keratinocytes contain cNOS, mainly neuronal NOS, which is activated by

[*]Corresponding author: wus1@ohio.edu (Shiyong Wu).

UV-induced calcium flux (15–20). UV also induces iNOS expression with a maximized mRNA level at 24 h postirradiation in human skin (9,21). UV-induced $NO^{\cdot}$ production was shown to protect cultured keratinocytes and skin from apoptotic death (2,3,5,22,23). However, all the reported studies were based on indirect observation that the inhibition of NOS or supplementation of $NO^{\cdot}$ donor during a period of 18–24 h protected keratinocytes from apoptotic death. An elevation of $NO^{\cdot}$ was detected immediately after UV irradiation in endothelial and epithelial cells (18,24). The impact of the early release of $NO^{\cdot}$ on UV-induced apoptosis has not been studied yet. In this report, we used a direct method (electrochemical nanosensors) to measure simultaneously at real time, *in situ*, the $NO^{\cdot}$ and $ONOO^{-}$ release from cultured keratinocytes and skin tissue of mice after irradiation of UVB. We demonstrated that UVB generated high level of $ONOO^{-}$ shifts unfavorable $NO^{\cdot}$/$ONOO^{-}$ balance and has a pro-apoptotic effect on both cultured cells and living skin.

Materials and Methods

Animals

Adult BALB/c mice were housed in a pathogen-free barrier facility in accordance with the standards of Ohio University. Mice were kept in groups of two per cage in a 12 h light/12 h dark cycle and housed at 25°C and 50% relative humidity.

Cell culture

The immortalized human keratinocyte cell line HaCaT was kindly provided by Dr. Hongtao Yu (Jackson State University, MS). The cells were cultured as monolayer in DMEM (Cellgro) with 10% FBS (Cellgro) at 37°C with 5% CO_2.

Nanosensors for continuous measurement of $NO^{\cdot}$ and $ONOO^{-}$

Concurrent measurements of $NO^{\cdot}$ and $ONOO^{-}$ were performed with electrochemical nanosensors (300–500 nm diameter). The designs are based on previously developed and well-characterized chemically modified carbon-fiber technology (25–29). Each of the sensors was made by depositing a sensing material on the tip of the carbon fiber. We used a conductive film of polymeric nickel (II) tetrakis (3-methoxy-4hydroxy-phenyl) porphyrinic for the $NO^{\cdot}$ sensor (25,28,29) and a polymeric film of Mn (III)–paracyclophanyl-porphyrin for the $ONOO^{-}$ sensor (26,27). Amperometry was used to measure changes in $NO^{\cdot}$ and $ONOO^{-}$ concentrations from its basal level with time (detection limit of 1 n_M and resolution time <50 ms for each sensor). Linear calibration curves were constructed for each sensor from 5 n_M to 3 μ_M before and after measurements with aliquots of $NO^{\cdot}$ and $ONOO^{-}$ standard solutions, respectively.

Determination of UVB-induced $NO^{\cdot}$, and $ONOO^{-}$ production in a single cell

Cells were seeded at 10^3 cells cm^{-2} and cultured for 12 h in complete medium. The sensors were positioned near the surface (5 ± 2 μm) of a selected cell with the help of a computer-controlled micromanipulator. The background signals of $NO^{\cdot}$ and $ONOO^{-}$ were stabilized and the cells were exposed to UVB irradiation at a power of 0.5 mW cm^{-2}. The signals generated by the nanosensors were recorded continuously for 80 s.

Determination of UVB-induced $NO^{\cdot}$ and $ONOO^{-}$ production in living mouse skin

The back of mice was shaved with an electric clipper 1 day prior to the experiment. Under anesthesia (ketamine 50 mg kg^{-1} + xylazine 5 mg kg^{-1}), the module nanosensors (total diameter 3.0 ± 0.5 μm) were inserted into the epidermal and dermal layers. L-shaped carbon fibers with the tip sharpened in microwave plasma were used in this study. Computer-controlled micromanipulators with *x*,*y*,*z* resolution ±2 μm were employed to implant the

sensors in the skin. The *z* coordinate (depth) was calibrated using piezoelectric currents recorded at zero distance from the skin (electrode touching the skin). The productions of $NO^{\cdot}$ and $ONOO^{-}$ were continuously recorded. Once the background signals of $NO^{\cdot}$ and $ONOO^{-}$ were stabilized, the mice were UVB-irradiated at a power of 0.5 mW cm^{-2}. The productions of $NO^{\cdot}$ and $ONOO^{-}$ were continuously recorded for 40 s.

Inhibition of early release of $NO^{\cdot}$ and $ONOO^{-}$ in cultured cells and skin epidermis

An *N*-substituted L-arginine analog N^{G}-methyl-L-arginine (L-NMMA; Sigma) was used to inhibit NOS activity; the glutathione (GSH) synthesis precursor *N*-acetyl-L-cysteine (L-NAC; Sigma) was used to scavenge free radicals and superoxide dismutase attached to polyethylene glycol (PEG-SOD) was used to dismutate superoxide ($O_2^{\cdot -}$). The cells were pretreated with L-NMMA (100 μM) or L-NAC (25 mM) for 2 h and then UVB-irradiated (50 mJ cm^{-2}). Immediately after irradiation, the cells were cultured in fresh medium without the inhibitors until further analysis. The mice were administered an intraperitoneal injection of L-NMMA (10 mg kg^{-1}) or L-NAC (500 mg kg^{-1}) 1 h before UVB irradiation.

Determination of cell apoptosis and death by flow cytometry

At 24 h postirradiation, the cells were digested with 0.01% trypsin and combined with the cells floating in the medium. An Annexin V: FITC Apoptosis Detection Kit II (BD Pharmingen) was used following the manufacturer's protocol. The annexin V-fluorescein isothiocyanate (FITC)/propidium iodide (PI) stained cells were analyzed by using a FACSort Flow Cytometer (Becton Dickinson) equipped with Cell-Quest software (Becton Dickinson). The parameter of the measurement was set at SSC 350, FL1 700 and FL2 700, and a total 10 000 cells were counted.

Cell injury assay using calcium green-1 acetoxymethylester (CAG-AM) and PI fluorescence staining

At 1 h postirradiation, the cells were incubated with CAG-AM (2.5 μM; Invitrogen) and PI (50 μg mL^{-1}) for 30 min at room temperature. After washing three times with PBS, fluorescence images were acquired by a camera connected to a confocal microscope (LSM 510; Carl Zeiss) at excitation and emission wavelengths of 506/531 nm for calcium green-1 and 535/617 nm for PI, respectively.

Analysis of membrane damage in mice epidermis

At 24 h before UVB exposure, mice were shaved with electric clippers. Non-UVB-treated controls were also shaved to maintain a constant protocol. The mice were anesthetized with Avertin and treated with the chemical and/or UVB (100 mJ cm^{-2}). Immediately after irradiation, the mice were injected subcutaneously with 0.1 mL of PI (100 μg mL^{-1}; Sigma). Thirty minutes after PI injection, the mice were euthanized by decapitation and skin tissue was harvested and sliced with a cryostat section in 40 nm thickness. The fluorescent images were acquired by a camera connected to a Nikon fluorescent microscope at excitation and emission wavelengths of 535 and 617 nm, respectively. The intensity of the PI staining was analyzed using ImageJ (v1.42k; NIH).

Western blotting

HaCaT cells were treated with L-NMMA and L-NAC for 2 h before UVB irradiation. At 24 h post-UVB, the cells were lysed at 4°C in NP-40 lysis buffer (2% NP-40, 80 mM NaCl, 100 mM Tris-HCl, 0.1% SDS) containing a Proteinase Inhibitor Cocktail (Complete™; Roche Molecular Biochemicals). The protein samples were then added to five-fold Laemmli buffer (0.32 M Tris-HCl, pH 6.8, 0.5 M glycine, 10% SDS, 50% glycerol and 0.03% bromophenol blue) and boiled. These samples were separated on an SDS-PAGE gel and then transferred

onto a nitrocellulose membrane. The membrane was blocked with 5% (wt/vol) skim milk in TBST (20 mM Tris [pH 7.5], 150 mM NaCl, 0.1% Tween 20) for 1 h and then incubated with anti-poly(ADP-ribose) polymerase (anti-PARP) antibodies (obtained from Santa Cruz Biotechnology) at 4°C overnight. After washing with TBST, the membrane was incubated with HRP-conjugated anti-rabbit antibody for 1 h at room temperature. The membrane was then washed three times in TBST and two times in TBS, and developed in West Pico Supersignal chemiluminescent substrate (Pierce).

UVB irradiation

UVB was generated from an 8 or 15 W UVB lamp (UVP). The intensity of UVB was standardized by an UVB-meter (UVP). The media was replaced with PBS during the irradiation. After UVB irradiation, fresh medium added to each plate was used in the experiments.

Statistical analysis

Student's *t*-test was used to analyze the significance of data. $P < 0.05$ was considered significant.

Results

UVB induces release of $NO^{\cdot}$ and $ONOO^{-}$ in cultured human keratinocytes

$NO^{\cdot}$ can rapidly react with $O_2^{\cdot -}$ to form $ONOO^{-}$ (30,31), a highly oxidative molecule (32). To determine the biological property of $NO^{\cdot}$ after UV irradiation, we measured the realtime production of $NO^{\cdot}$ and $ONOO^{-}$ in UVB-treated HaCaT by using a $NO^{\cdot}$ or $ONOO^{-}$ nanosensor. After positioning the nanosensors near the surface of keratinocytes (5 ± 2 μm), the productions of $NO^{\cdot}$ or $ONOO^{-}$ were continuously monitored. Our data showed that 4 s after the exposure of the keratinocytes to UVB, a rapid release of $ONOO^{-}$ was observed (Fig. 1A). A maximal $[ONOO^{-}]$ of 190 ± 20 was reached after 15 ± 2 s postradiation (Fig. 1A,B). $NO^{\cdot}$ release was recorded after 20 ± 2 s and reached a maximal level of 91 ± 8 nM at 40 ± 5 s postradiation (Fig. 1A,B). These results suggest that the cells were under high oxidative stress when $NO^{\cdot}$ was just released after UVB irradiation.

To determine maximal concentrations of $NO^{\cdot}$ and $ONOO^{-}$ in the keratinocytes, we measured $NO^{\cdot}/ONOO^{-}$ after stimulation of cNOS with the calcium-independent agonist, CaI. The kinetics of CaI-stimulated $ONOO^{-}$ and $NO^{\cdot}$ release was distinctively different from that observed after UVB stimulation (Fig. 1C vs 1A). A rapid increase in $[NO^{\cdot}]$ was observed after less than 0.1 s after treatment of CaI. The maximal $[NO^{\cdot}]$ (195 ± 15 nM) was reached about 1.0 ± 0.1 s postinjection of CaI. The release of $NO^{\cdot}$ was followed by the release of $ONOO^{-}$ (0.3 ± 0.1 s after treatment of CaI), which reached a maximum of 90 ± 10 nM after 1.2 ± 0.1 s. A ratio of $[NO^{\cdot}]/[ONOO^{-}]$ was used to quantify a level of oxidative/nitroxidative stress and $NO^{\cdot}/ONOO^{-}$ imbalance in keratinocytes after stimulation with UVB or CaI (Fig. 1B,D). High $[NO^{\cdot}]/[ONOO^{-}]$ ratio indicates high concentration of bioavailable, cytoprotective $NO^{\cdot}$ and/or low levels of cytotoxic $ONOO^{-}$. The ratio of $[NO^{\cdot}]/[ONOO^{-}]$ was 0.42 ± 0.05 after stimulation of keratinocytes with UVB radiation and 2.15 ± 0.10 after stimulation with CaI. These results suggest that there is a rapid increase in $O_2^{\cdot -}$, which reacts with $NO^{\cdot}$ to form $ONOO^{-}$ after UVB irradiation.

To confirm that the UVB-induced elevation of $O_2^{\cdot -}$ leads to the imbalance of $[NO^{\cdot}]/[ONOO^{-}]$, we analyzed the production of $[NO^{\cdot}]$ and $[ONOO^{-}]$ in the presence of the cNOS inhibitor L-NAME and a membrane-permeable superoxide dismutase PEG-SOD. In the presence of L-NAME, both $[NO^{\cdot}]$ and $[ONOO^{-}]$ decreased significantly (Fig. 2). However, the decrease in $NO^{\cdot}$ was more pronounced (about 85%) than the decrease in $ONOO^{-}$ (about

70%). An incubation of keratinocytes with PEG-SOD increased the $NO^{\cdot}$ level to 165 ± 15 n_M (80% increase *vs* control) while $ONOO^-$ level decreased by about 30% compared to control. $[NO^{\cdot}]/[ONOO^-]$ ratio did not change significantly in the presence of L-NAME and increased significantly in the presence of PEG-SOD (Fig. 2B). These results demonstrate that UVB-induced production of $NO^{\cdot}$ was accompanied by an elevation of $O_2^{\cdot -}$, most likely due to photolytic reaction of oxygen and/or $O_2^{\cdot -}$ production by uncoupled cNOS.

UVB induces $NO^{\cdot}$ and $ONOO^-$ production in skin epidermis *in vivo*

After quantitatively analyzing $NO^{\cdot}$ and $ONOO^-$ in cultured cells, we determined the UVB-induced release of $NO^{\cdot}$ and $ONOO^-$ in living mouse skin. The module nanosensors (total diameter 3.0 ± 0.5 μm) were inserted underneath the skin surface of the anesthetized mouse (Fig. 3A) and the productions of $NO^{\cdot}$ or $ONOO^-$ were continuously recorded (Fig. 3B) before and after the irradiation. Our data show that the exposure of the living skin to UVB causes a rapid release of $NO^{\cdot}$ and $ONOO^-$ at 4 s postirradiation. Interestingly, while the release of $ONOO^-$ rapidly reaches a maximum of 270 ± 20 n_M at 15 s postirradiation and slowly reduced, the release of $NO^{\cdot}$ remains raising to 150 ± 8 n_M at the end of the measurement (Fig. 3B,C). Our results demonstrate that the patterns for the release of $NO^{\cdot}$ and $ONOO^-$ in response to UVB irradiation are distinctive in cultured cells and living skin (Fig. 3B *vs* 1A).

Early elevation of $NO^{\cdot}$ and oxidative stress mediates UVB-induced death of keratinocytes

As an elevation of $NO^{\cdot}$ could be pro- or anti-apoptotic (33), we determined whether this early release of $NO^{\cdot}$ in combination with $ONOO^-$ inhibits or promotes apoptosis of cultured HaCaT cells upon UVB irradiation. The cell death was analyzed using annexin V and PI double-staining to determine the loss of membrane phospholipid symmetry and membrane integrity (34,35). At 24 h postirradiation, the UVB-induced apoptotic cell death was reduced from 17.6 ± 1.7% to 14.4 ± 1.5% or 10.8 ± 1.0%, respectively, upon L-NMMA or L-NAC treatment (Fig. 4A). The effects of L-NMMA and L-NAC on UVB-induced cell death were also analyzed by determination of cleavage of poly (ADP-ribose) polymerase (PARP). Our data showed that UVB induced a cleavage of 116 kDa PARP to an 89-kDa fragment (Fig. 4B, lane 2 *vs* 1), which is the marker for cell apoptosis. Treating the cells with L-NMMA and L-NAC partially protected PARP cleavage upon UVB irradiation (Fig. 4B, lanes 3 and 4 *vs* lane 2 [correction added after online publication Jan 13 2010: lane 4 changed to lane 2]). Interestingly, treating the cells with L-NAC did not only reduce the PARP cleavage but also reduced the PARP expression after UVB irradiation (Fig. 4B, lane 4 *vs* lanes 1–3). The data agreed with our previous reports, which indicated that L-NAC protects eIF2α from UV-induced phosphorylation (36) and elimination of eIF2α phosphorylation reduces PARP expression after UV treatment (37).

In addition to apoptosis, we also determined whether the early release of $NO^{\cdot}$ initiates necrotic death of UVB-treated HaCaT cells. Necrosis is initiated due to injury to the cells, which could be characterized by the loss of membrane integrity (38). We analyzed membrane integrity using the PI staining method. The living cells were stained and visualized by using CAG-AM staining. Our data show that UVB irradiation induces a loss of membrane integrity in the cells within 1 h of treatment (Fig. 4C, column 2 *vs* 1). The inhibition of NOS or free radicals significantly reduces the amount of injured cells (Fig. 5B, columns 3 and 4 *vs* 2). Our results demonstrate that the early release of $NO^{\cdot}$ and $ONOO^-$ mediates UVB-induced apoptotic and necrotic death of cells.

UVB-induced elevation of $NO^{\cdot}$ and oxidative stress leads to tissue damage

To assess the role of NOS and oxidative stress in UVB-induced skin injury, we analyzed the effect of L-NMMA and L-NAC on UVB-induced loss of membrane integrity in living mice

skin tissue. Compared to the samples from the UVB-irradiated mice, the skin tissue harvested from the mice with L-NMMA showed a significant decrease in fluorescence intensity in the epidermis (Fig. 5), which consists of 90–95% of keratinocytes. The treatment of L-NAC almost totally inhibited UVB-induced tissue injury (Fig. 5). These results demonstrated that UVB-induced rapid activation of NOS in combination with oxidative stress led to the loss of membrane integrity and skin injury.

Discussion

UVB induces a rapid release of $NO^{\cdot}$ and $O_2^{\cdot -}$ in cultured keratinocytes (24). However, the formation of the more reactive $ONOO^-$ has never been directly measured after UVB irradiation. Furthermore, the effect of UVB radiation on $NO^{\cdot}$ production in the skin has been assessed only with the use of indirect methods (39). Indirect measurements cannot separate an effect of $NO^{\cdot}$ in biological milieu from the effect of $ONOO^-$. In this study we used highly sensitive, selective, millisecond response-time electrochemical nanosensors (40) to directly measure the concentration of UVB- and CaI-stimulated $NO^{\cdot}$ and $ONOO^-$ release in cultured keratinocytes and in the epidermis of mice.

Our results demonstrate that a short-time exposure of cultured keratinocytes or the epidermis of mice to UVB irradiation stimulated $NO^{\cdot}$ release as well as $ONOO^-$ production (Figs. 1 and 3). The study of NOS activity showed dependence upon calcium, indicating the involvement of the cNOS rather than the iNOS in $NO^{\cdot}/ONOO^-$ production (Fig. 2). As the crucial role of $NO^{\cdot}$ in the physiology of vasculature has become well established, the question arises whether $NO^{\cdot}$ directly or indirectly, through the formation of more reactive oxidative species such as $ONOO^-$, averts its deleterious biological effects. It is interesting to note that the UVB-induced $ONOO^-$ release in cultured keratinocytes precedes the production of bioavailable (diffusible) $NO^{\cdot}$ (Fig. 1). This is in contrast to calcium-stimulated $NO^{\cdot}$ release where the generation of $ONOO^-$ follows the production of $NO^{\cdot}$ (Fig. 2). To explain the differences in the effect of UVB on $NO^{\cdot}$ production *vs* $ONOO^-$ production, it may help to realize that the $NO^{\cdot}$ sensor used in this study detects the net concentration of $NO^{\cdot}$ (*i.e.* $NO^{\cdot}$ that is not consumed in fast chemical reactions and can freely diffuse to a target cell and trigger cGMP production). This net concentration depends not only on the activity of eNOS but also on the production of $O_2^{\cdot -}$. $NO^{\cdot}$ rapidly reacts with $O_2^{\cdot -}$ in diffusion-controlled reactions ($k = 6 \times 10^{10}$ $nmol^{-1}s^{-1}$) to form $ONOO^-$. There are several potential sources of $O_2^{\cdot -}$ in cells including NAD(P)H, cNOS, mitochondria and others. It is also well established that UVB induces $O_2^{\cdot -}$ production (24,41). UVB exposure generates $O_2^{\cdot -}$ immediately after the exposure, and the reactive oxygen species thus produced remains for 100–1200 s. The data presented here indicate that initially produced $ONOO^-$ is most likely a result of the reaction between $O_2^{\cdot -}$ generated by photolytic reduction of oxygen and $NO^{\cdot}$ generated by uncoupled cNOS. $ONOO^-$ is formed when $NO^{\cdot}$ and $O_2^{\cdot -}$ react in a fast ($k = 2 \times 10^{10}$ $mol^{-1}s^{-1}$) reaction (30,31). Formation of $ONOO^-$ is favored by the overproduction of $O_2^{\cdot -}$ and/or $NO^{\cdot}$.

After measuring the kinetics of $NO^{\cdot}$ and $ONOO^-$ productions, we determined the role of the early cNOS activation and $NO^{\cdot}/ONOO^-$ imbalance in UVB-induced apoptosis by analyzing Annexin V-FITC/PI double-stained cells or PARP cleavage. L-NAC, a commonly used $ONOO^-$ reducer (36,42,43), was used to increase the ratio of $NO^{\cdot}/ONOO^-$. Our data showed that preincubation of the cells with either an NOS inhibitor or an antioxidant reduced apoptotic death of the UVB-treated cells (Fig. 4). These results suggest that the early $NO^{\cdot}$ release enhances oxidative stress-induced apoptosis upon UVB irradiation. The UVB-induced apoptosis is likely to be trigged by the oxidative damage to the cell membrane at the early stage of irradiation. $NO^{\cdot}$ is an unstable molecule, which rapidly reacts with $O_2^{\cdot -}$ to form $ONOO^-$ and its protonated form (ONOOH). $ONOO^-$ is a potent inducer of

apoptosis (44,45). While [$O_2^{\cdot -}$] is low, $ONOO^-$ can isomerize to harmless NO_3^-. However, at high [$O_2^{\cdot -}$], $ONOO^-$ undergoes a hemolytic or heterolytic cleavage to form strong oxidants including $HO^{\cdot -}$, NO_2^- and NO_2^+. These species initiate a cascade of events leading to an increase in cytotoxicity and trigger cellular damage. In UVB-treated cells, high levels of $O_2^{\cdot -}$ can be generated by reduction of O_2, by uncoupled eNOS or by other sources like NADP(H) oxidase. However, the most effective generator of $O_2^{\cdot -}$ is uncoupled cNOS (46). Our data showed that the early activation of cNOS led to an injury of the cultured cells and skin tissue within 1 h postirradiation (Figs. 4C and 5). The UVB-induced membrane damage of cells or skin tissue could be reduced or prevented by pretreatment of L-NMMA or L-NAC (Figs. 4C and 5). Furthermore, the early membrane damage correlated with the late apoptosis of the irradiated cells. These results suggest that UVB-induced apoptosis could be trigged by an early-induced $NO^{\cdot}$ release in combination with high production of $O_2^{\cdot -}$. Based on our results, we propose a novel model (Fig. 6) that UVB induced immediate activation of cNOS and production of $NO^{\cdot}$, which rapidly reacts with $O_2^{\cdot -}$ to form $ONOO^-$, which induces oxidative membrane damage and apoptosis of the irradiated cells.

Acknowledgments

This work is partially supported by R56 CA86928 (to S.W.) and RO1 CA086928 (to S.W.).

References

1. Oplander C, Cortese MM, Korth HG, Kirsch M, Mahotka C, Wetzel W, Pallua N, Suschek CV. The impact of nitrite and antioxidants on ultraviolet-A-induced cell death of human skin fibroblasts. Free Radic Biol Med 2007;43:818–829. [PubMed: 17664145]
2. Suschek CV, Briviba K, Bruch-Gerharz D, Sies H, Kroncke KD, Kolb-Bachofen V. Even after UVA-exposure will nitric oxide protect cells from reactive oxygen intermediate-mediated apoptosis and necrosis. Cell Death Differ 2001;8:515–527. [PubMed: 11423912]
3. Suschek CV, Krischel V, Bruch-Gerharz D, Berendji D, Krutmann J, Kronckei KD, Kolb-Bachofen V. Nitric oxide fully protects against UVA-induced apoptosis in tight correlation with Bcl-2 up-regulation. J Biol Chem 1999;274:6130–6137. [PubMed: 10037696]
4. Weller R, Billiar T, Vodovotz Y. Pro- and anti-apoptotic effects of nitric oxide in irradiated keratinocytes: The role of superoxide. Skin Pharmacol Appl Skin Physiol 2002;15:348–352. [PubMed: 12239430]
5. Yamaoka J, Kawana S, Miyachi Y. Nitric oxide inhibits ultraviolet B-induced murine keratinocyte apoptosis by regulating apoptotic signaling cascades. Free Radic Res 2004;38:943–950. [PubMed: 15621712]
6. Madajka M, Korda M, White J, Malinski T. Effect of aspirin on constitutive nitric oxide synthase and the biovailability of NO. Thromb Res 2003;110:317–321. [PubMed: 14592555]
7. Newman E, Spratt DE, Mosher J, Cheyne B, Montgomery HJ, Wilson DL, Weinberg JB, Smith SM, Salerno JC, Ghosh DK, Guillemette JG. Differential activation of nitric-oxide synthase isozymes by calmodulin-troponin C chimeras. J Biol Chem 2004;279:33547–33557. [PubMed: 15138276]
8. Zhang ZG, Chopp M, Bailey F, Malinski T. Nitric oxide changes in the rat brain after transient middle cerebral artery occlusion. J Neurol Sci 1995;128:22–27. [PubMed: 7536815]
9. Kuhn A, Fehsel K, Lehmann P, Krutmann J, Ruzicka T, Kolb-Bachofen V. Aberrant timing in epidermal expression of inducible nitric oxide synthase after UV irradiation in cutaneous lupus erythematosus. J Invest Dermatol 1998;111:149–153. [PubMed: 9665402]
10. Arany I, Brysk MM, Brysk H, Tyring SK. Regulation of inducible nitric oxide synthase mRNA levels by differentiation and cytokines in human keratinocytes. Biochem Biophys Res Commun 1996;220:618–622. [PubMed: 8607813]
11. Qureshi AA, Hosoi J, Xu S, Takashima A, Granstein RD, Lerner EA. Langerhans cells express inducible nitric oxide synthase and produce nitric oxide. J Invest Dermatol 1996;107:815–821. [PubMed: 8941667]

12. Wang R, Ghahary A, Shen YJ, Scott PG, Tredget EE. Human dermal fibroblasts produce nitric oxide and express both constitutive and inducible nitric oxide synthase isoforms. J Invest Dermatol 1996;106:419–427. [PubMed: 8648170]
13. Rocha IM, Guillo LA. Lipopolysaccharide and cytokines induce nitric oxide synthase and produce nitric oxide in cultured normal human melanocytes. Arch Dermatol Res 2001;293:245–248. [PubMed: 11409569]
14. Tsatmali M, Manning P, McNeil CJ, Thody AJ. alpha-MSH inhibits lipopolysaccharide induced nitric oxide production in B16 mouse melanoma cells. Ann N Y Acad Sci 1999;885:474–476. [PubMed: 10816692]
15. Deliconstantinos G, Villiotou V, Stavrides JC. Nitric oxide and peroxynitrite released by ultraviolet B-irradiated human endothelial cells are possibly involved in skin erythema and inflammation. Exp Physiol 1996;81:1021–1033. [PubMed: 8960707]
16. Deliconstantinos G, Villiotou V, Stravrides JC. Release by ultraviolet B (u.v.B) radiation of nitric oxide (NO) from human keratinocytes: A potential role for nitric oxide in erythema production. Br J Pharmacol 1995;114:1257–1265. [PubMed: 7620717]
17. Ignarro LJ, Buga GM, Wood KS, Byrns RE, Chaudhuri G. Endothelium-derived relaxing factor produced and released from artery and vein is nitric oxide. Proc Natl Acad Sci USA 1987;84:9265–9269. [PubMed: 2827174]
18. Kubaszewski E, Peters A, McClain S, Bohr D, Malinski T. Light-activated release of nitric oxide from vascular smooth muscle of normotensive and hypertensive rats. Biochem Biophys Res Commun 1994;200:213–218. [PubMed: 8166690]
19. Marletta MA. Nitric oxide: Biosynthesis and biological significance. Trends Biochem Sci 1989;14:488–492. [PubMed: 2696179]
20. Nathan C. Inducible nitric oxide synthase: What difference does it make? J Clin Invest 1997;100:2417–2423. [PubMed: 9366554]
21. Meeran SM, Katiyar N, Singh T, Katiyar SK. Loss of endogenous interleukin-12 activates survival signals in ultraviolet-exposed mouse skin and skin tumors. Neoplasia 2009;11:846–855. [PubMed: 19724678]
22. Fukunaga-Takenaka R, Fukunaga K, Tatemichi M, Ohshima H. Nitric oxide prevents UV-induced phosphorylation of the p53 tumor-suppressor protein at serine 46: A possible role in inhibition of apoptosis. Biochem Biophys Res Commun 2003;308:966–974. [PubMed: 12927814]
23. Schneiderhan N, Budde A, Zhang Y, Brune B. Nitric oxide induces phosphorylation of p53 and impairs nuclear export. Oncogene 2003;22:2857–2868. [PubMed: 12771937]
24. Aitken GR, Henderson JR, Chang SC, McNeil CJ, Birch-Machin MA. Direct monitoring of UV-induced free radical generation in HaCaT keratinocytes. Clin Exp Dermatol 2007;32:722–727. [PubMed: 17953641]
25. Brovkovych V, Patton S, Brovkovych S, Kiechle F, Huk I, Malinski T. In situ measurement of nitric oxide, superoxide and peroxynitrite during endotoxemia. J Physiol Pharmacol 1997;48:633–644. [PubMed: 9444612]
26. Kalinowski L, Dobrucki LW, Szczepanska-Konkel M, Jankowski M, Martyniec L, Angielski S, Malinski T. Third-generation beta-blockers stimulate nitric oxide release from endothelial cells through ATP efflux: A novel mechanism for antihypertensive action. Circulation 2003;107:2747–2752. [PubMed: 12742996]
27. Kalinowski L, Malinski T. Endothelial NADH/-NADPH-dependent enzymatic sources of superoxide production: Relationship to endothelial dysfunction. Acta Biochim Pol 2004;51:459–469. [PubMed: 15218542]
28. Malinski T, Radomski MW, Taha Z, Moncada S. Direct electrochemical measurement of nitric oxide released from human platelets. Biochem Biophys Res Commun 1993;194:960–965. [PubMed: 8343175]
29. Malinski T, Taha Z. Nitric oxide release from a single cell measured in situ by a porphyrinic-based microsensor. Nature 1992;358:676–678. [PubMed: 1495562]
30. Beckman JS, Koppenol WH. Nitric oxide, superoxide, and peroxynitrite: The good, the bad, and ugly. Am J Physiol 1996;271:C1424–C1437. [PubMed: 8944624]

31. Groves JT. Peroxynitrite: Reactive, invasive and enigmatic. Curr Opin Chem Biol 1999;3:226–235. [PubMed: 10226050]
32. Pataer A, Vorburger SA, Barber GN, Chada S, Mhashilkar AM, Zou-Yang H, Stewart AL, Balachandran S, Roth JA, Hunt KK, Swisher SG. Adenoviral transfer of the melanoma differentiation-associated gene 7 (mda7) induces apoptosis of lung cancer cells via up-regulation of the double-stranded RNA-dependent protein kinase (PKR). Cancer Res 2002;62:2239–2243. [PubMed: 11956076]
33. Snyder SH. Janus faces of nitric oxide. Nature 1993;364:577. [PubMed: 8102475]
34. Schindl A, Klosner G, Honigsmann H, Jori G, Calzavara-Pinton PC, Trautinger F. Flow cytometric quantification of UV-induced cell death in a human squamous cell carcinoma-derived cell line: Dose and kinetic studies. J Photochem Photobiol B, Biol 1998;44:97–106.
35. Vermes I, Haanen C, Steffens-Nakken H, Reutelingsperger C. A novel assay for apoptosis. Flow cytometric detection of phosphatidylserine expression on early apoptotic cells using fluorescein labelled Annexin V. J Immunol Methods 1995;184:39–51. [PubMed: 7622868]
36. Lu W, Laszlo CF, Miao Z, Chen H, Wu S. The role of nitric oxide synthase in regulation of ultraviolet light-induced phosphorylation of the alpha-subunit of eukaryotic initiation factor 2. J Biol Chem 2009;284(36):24281–24288. [PubMed: 19586904]
37. Parker SH, Parker TA, George KS, Wu S. The roles of translation initiation regulation in ultraviolet light-induced apoptosis. Mol Cell Biochem 2006;293:173–181. [PubMed: 16786187]
38. Darzynkiewicz Z, Juan G, Li X, Gorczyca W, Murakami T, Traganos F. Cytometry in cell necrobiology: Analysis of apoptosis and accidental cell death (necrosis). Cytometry 1997;27:1–20. [PubMed: 9000580]
39. Virag L, Szabo E, Bakondi E, Bai P, Gergely P, Hunyadi J, Szabo C. Nitric oxide-peroxynitrite-poly(ADP-ribose) polymerase pathway in the skin. Exp Dermatol 2002;11:189–202. [PubMed: 12102657]
40. Heeba G, Moselhy M, Hassan M, Khalifa M, Gryglewski R, Malinski T. Anti-atherogenic effect of statins: Role of nitric oxide, peroxynitrite and haem oxygenase-1. Br J Pharmacol 2009;156(8):1256–1266. [PubMed: 19226281]
41. Hakozaki T, Date A, Yoshii T, Toyokuni S, Yasui H, Sakurai H. Visualization and characterization of UVB-induced reactive oxygen species in a human skin equivalent model. Arch Dermatol Res 2008;300(Suppl 1):S51–S56. [PubMed: 17968570]
42. Failli P, Palmieri L, D'Alfonso C, Giovannelli L, Generini S, Rosso AD, Pignone A, Stanflin N, Orsi S, Zilletti L, Matucci-Cerinic M. Effect of *N*-acetyl-l-cysteine on peroxynitrite and superoxide anion production of lung alveolar macrophages in systemic sclerosis. Nitric Oxide 2002;7:277–282. [PubMed: 12446176]
43. Lin KT, Xue JY, Sun FF, Wong PY. Reactive oxygen species participate in peroxynitrite-induced apoptosis in HL-60 cells. Biochem Biophys Res Commun 1997;230:115–119. [PubMed: 9020024]
44. Brune B, von Knethen A, Sandau KB. Nitric oxide (NO): An effector of apoptosis. Cell Death Differ 1999;6:969–975. [PubMed: 10556974]
45. Dimmeler S, Zeiher AM. Nitric oxide and apoptosis: Another paradigm for the double-edged role of nitric oxide. Nitric Oxide 1997;1:275–281. [PubMed: 9441899]
46. Huk I, Nanobashvili J, Neumayer C, Punz A, Mueller M, Afkhampour K, Mittlboeck M, Losert U, Polterauer P, Roth E, Patton S, Malinski T. L-arginine treatment alters the kinetics of nitric oxide and superoxide release and reduces ischemia / reperfusion injury in skeletal muscle. Circulation 1997;96:667–675. [PubMed: 9244241]

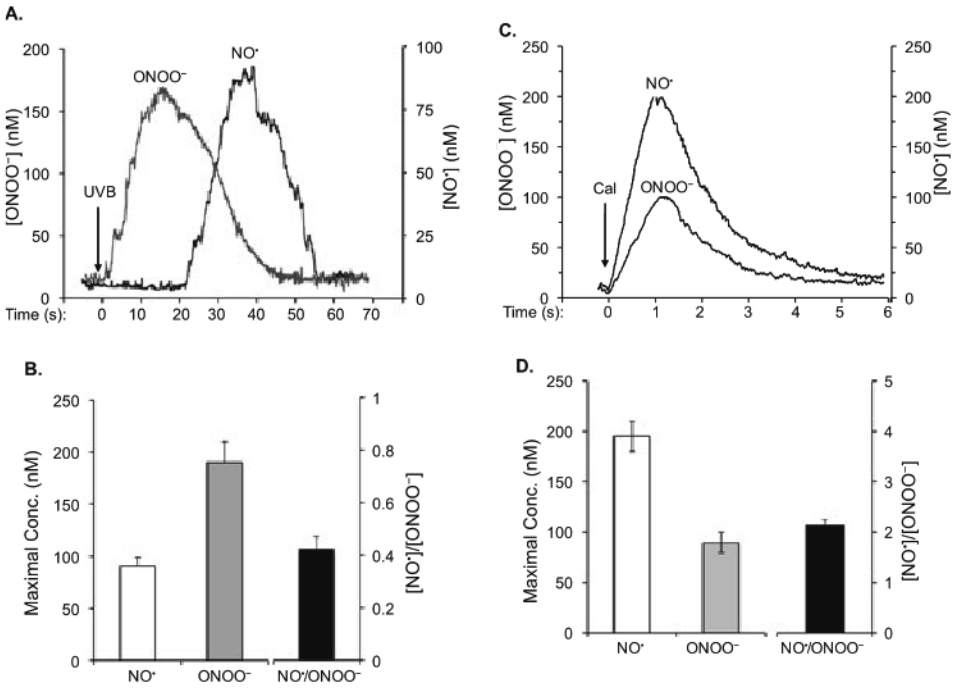

Figure 1.

$NO^{\cdot}$ and $ONOO^{-}$ amperograms (current calibrated as concentration *vs* time) and maximal $[NO^{\cdot}]$, $[ONOO^{-}]$ and a ratio of $[NO^{\cdot}]/[ONOO^{-}]$ measured in a keratinocyte after UVB irradiation. (A) Amperograms of $NO^{\cdot}$ and $ONOO^{-}$ release from the cells irradiated with UVB for 1 min at 0.5 mW cm^{-2}. (B) Maximal $[NO^{\cdot}]$, $[ONOO^{-}]$ and a ratio of maximal $[NO^{\cdot}]/[ONOO^{-}]$ produced by a keratinocyte after treating with UVB. (C) Amperograms of $NO^{\cdot}$ and $ONOO^{-}$ release from the cells stimulated by CaI (1 μ_M) in 6 s. (D) Maximal $[NO^{\cdot}]$, $[ONOO^{-}]$ and a ratio of maximal $[NO^{\cdot}]/[ONOO^{-}]$ produced by a keratinocyte after treating with CaI. The data in (B) and (D) represent the average of three sets of independent measurements.

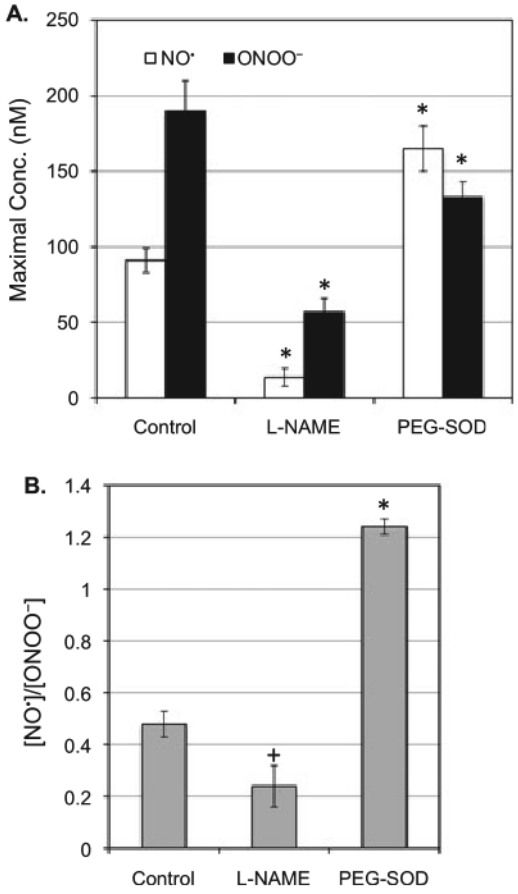

Figure 2.

$NO^{\cdot}$ and $ONOO^{-}$ release from the cells irradiated with UVB (0.5 mW cm^{-2}) for 1 min in the presence or absence of L-NAME (2 μ_M) or PEG-SOD (100 U). (A) Maximal [$NO^{\cdot}$] and [$ONOO^{-}$] produced by a keratinocyte after UVB treatment. (B) A ratio of maximal [$NO^{\cdot}$]/[$ONOO^{-}$] produced by a keratinocyte after UVB treatment. The data represent the average of three sets of independent measurements. *$P < 0.001$ *vs* control; + $P < 0.1$ *vs* control.

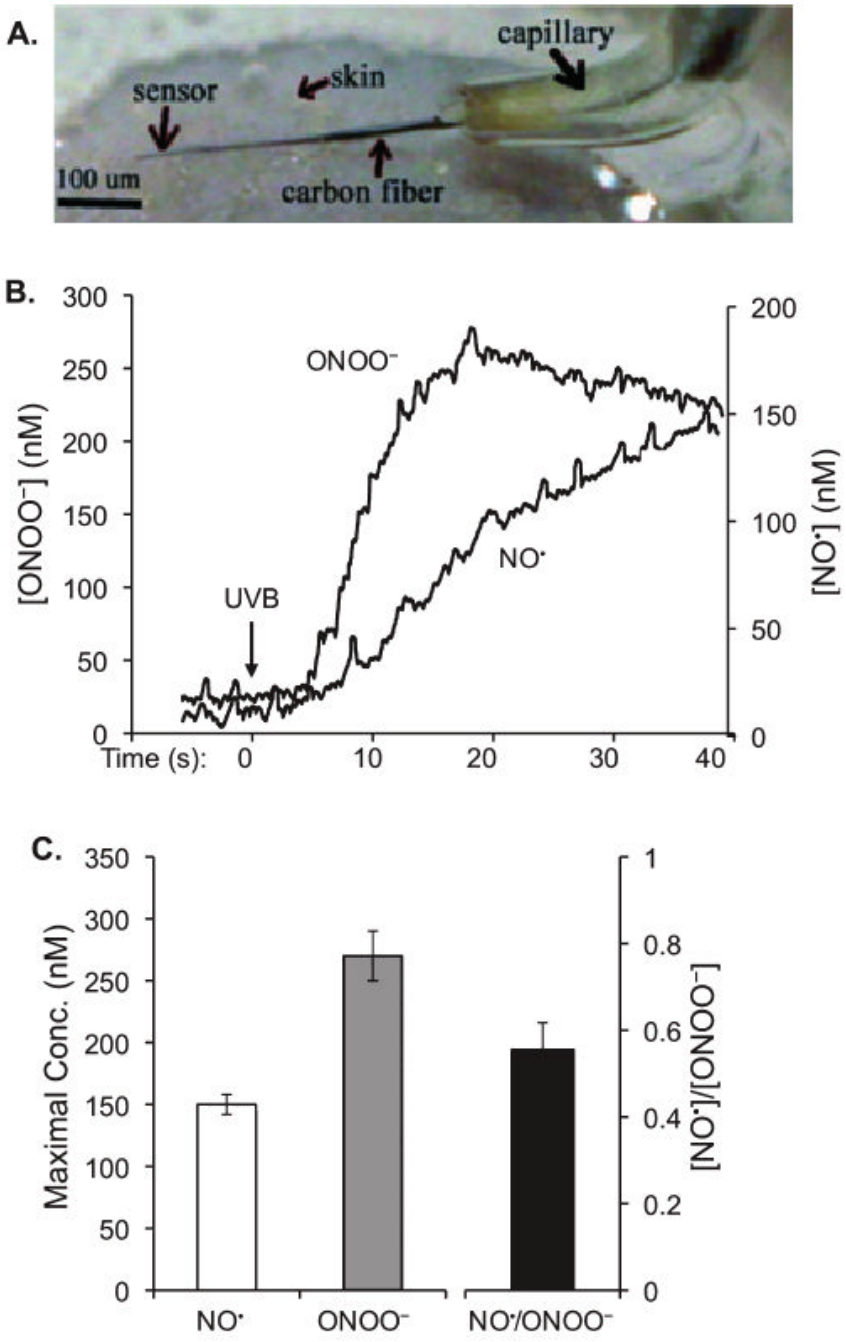

Figure 3.

In vivo measurement of $NO^{\cdot}$ and $ONOO^{-}$ in UVB-irradiated mouse skin using a nanosensor. (A) A micrograph of L-shaped sharpened carbon fibers with a module of $NO^{\cdot}$ and $ONOO^{-}$ sensors deposited at the tip of the carbon fibers. The module was implanted in the skin of a mouse. (B) Maximal [$NO^{\cdot}$], [$ONOO^{-}$] and a ratio of maximal [$NO^{\cdot}$]/[$ONOO^{-}$] produced by the irradiated skin. (C) Maximal [$NO^{\cdot}$], [$ONOO^{-}$] and a ratio of maximal [$NO^{\cdot}$]/[$ONOO^{-}$] produced by a keratinocyte after UVB treatment. The data represent the average of three sets of independent measurements.

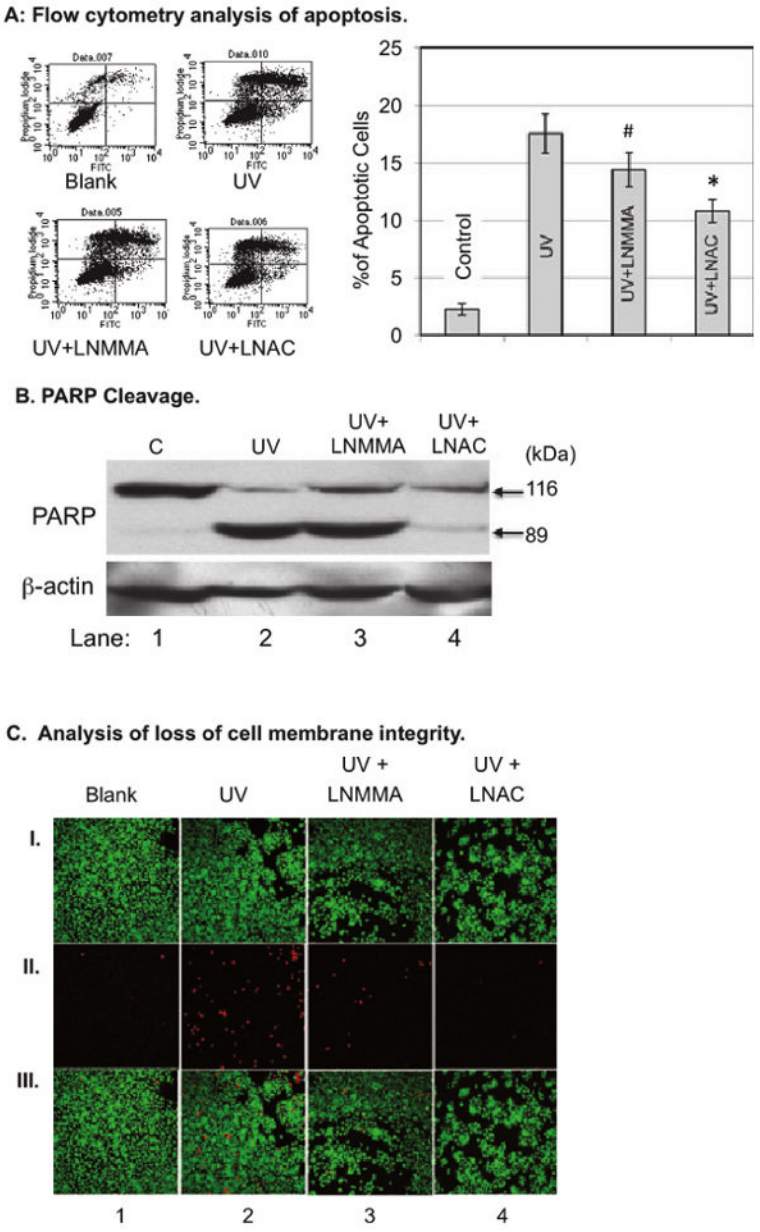

Figure 4.

HaCaT cells were treated with L-NMMA (100 μm) or L-NAC (25 mM) for 2 h and then irradiated with UVB (50 mJ cm^{-2}). (A) The cells were double-stained with Annexin V/PI at 24 h postirradiation. The percentages of apoptotic cells were determined by flow cytometric analysis. The data represent the average of three sets of independent measurements. #$P <$ 0.01 *vs* UVB alone; *$P < 0.005$ *vs* UVB alone. (B) The cells were lyzed at 24 h postirradiation and Western blot analysis was used to determine the PARP cleavage. (C) The cells were double-stained with CAG/PI at 1 h postirradiation. The images were captured by fluorescence confocal microscopy. (I) Living cells stained by CAG-AM (2.5 μM). (II) Injured cells that lost membrane integrity were stained with PI (50 μg mL^{-1}). (III) Pictures (I) and (II) overlaid on top of each other.

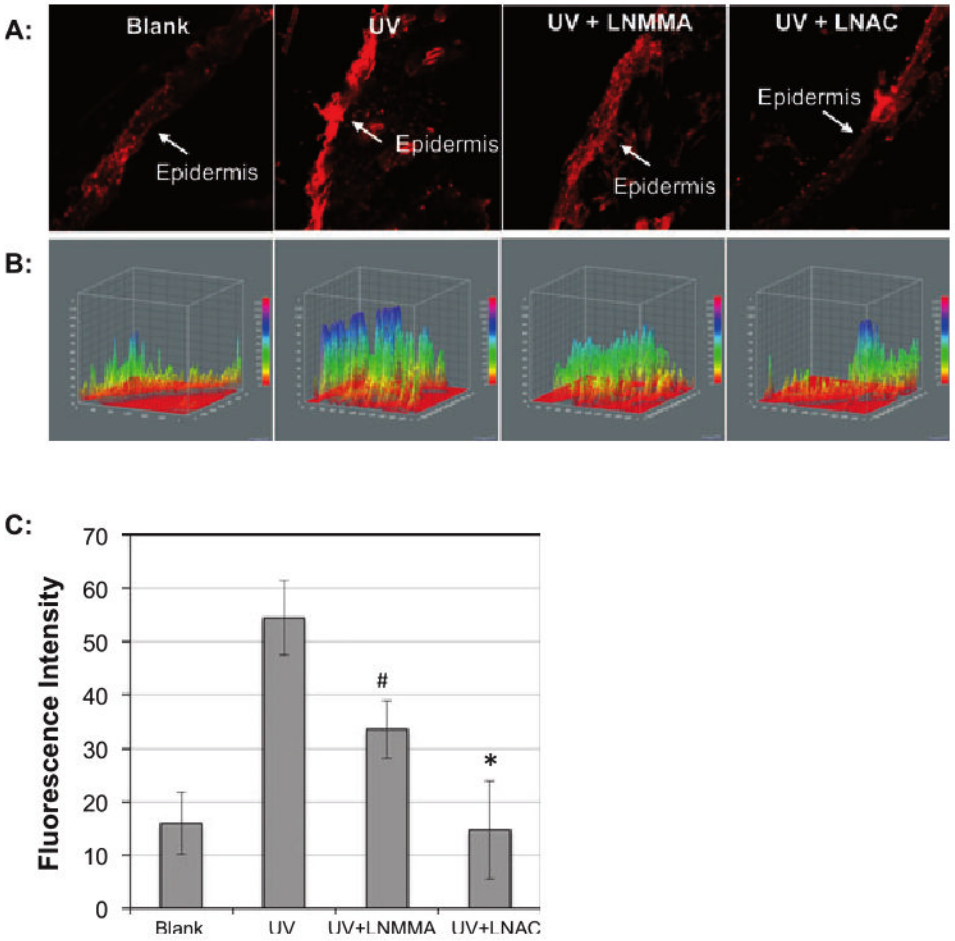

Figure 5.

PI staining was used to determine the UVB-induced injury of skin tissue of mice. The mice were injected intraperitoneally with L-NMMA (10 mg kg^{-1}) or L-NAC (500 mg kg^{-1}) at 1 h before UVB irradiation. Immediately after irradiation, the mice were injected subcutaneously with 0.1 mL PI (100 μg mL^{-1}) and the skin tissues were collected at 30 min postirradiation. The images of the skin sections were captured by fluorescence microscope. (A) Images of the PI-stained skin slices. (B) A 3-D analysis of the fluorescence intensity of the PI staining skin tissue using ImageJ (v1.34k; NIH). The fluorescence intensity is analyzed against distance of the slice in two dimensions. (C) The average fluorescence intensity of three measurements. #$P < 0.01$ *vs* UVB alone; *$P < 0.02$ *vs* UVB alone.

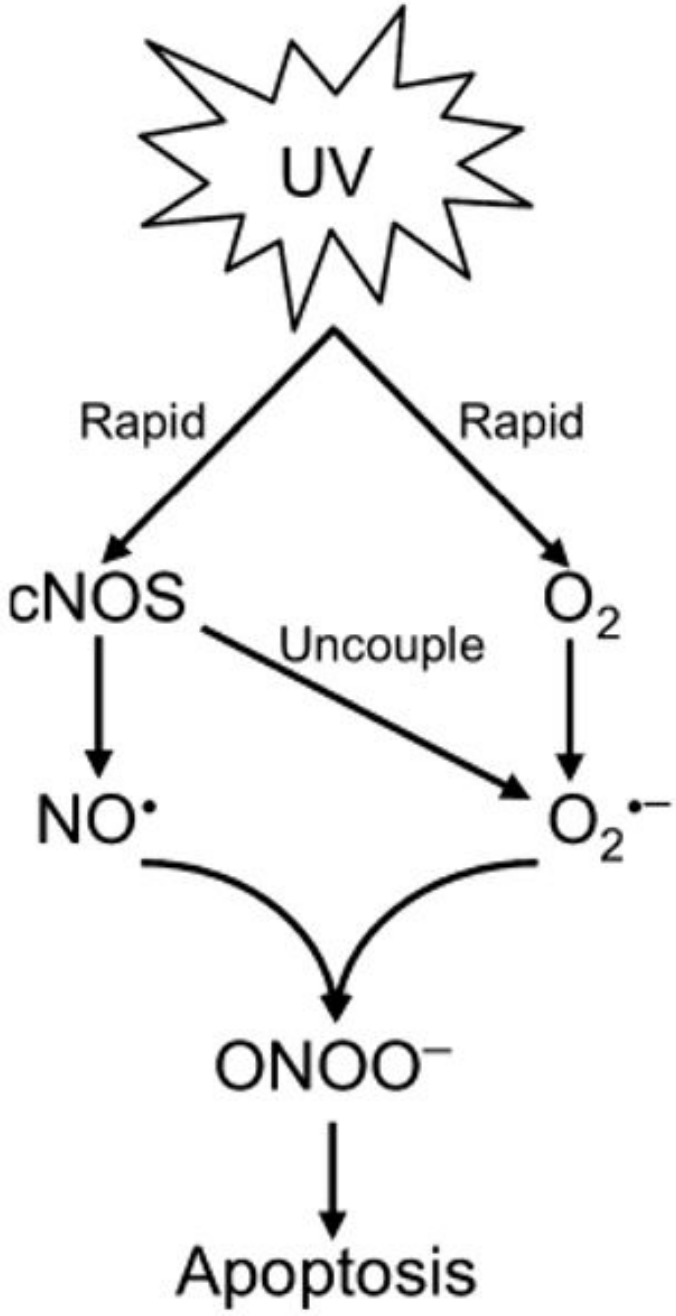

Figure 6.
Model of UVB-induced and NO˙-enhanced apoptotic signaling pathways.